ANALYTIC METHODS FOR TACTICAL AIR WARFARE

AIR CAMPAIGN AND HIGH-ENERGY LASER PROPAGATION ANALYSES

REPORT PA304T1

David Lee
Robert Hemm
Scott Houser
John Dukovich
Jeremy Eckhause
Dou Long

LMI
GOVERNMENT CONSULTING

SEPTEMBER 2004

REPORT DOCUMENTATION PAGE

Form Approved
OPM No.0704-0188

1. AGENCY USE ONLY *(Leave Blank)*	2. REPORT DATE	3. REPORT TYPE AND DATES COVERED
	September 2004	Final

4. TITLE AND SUBTITLE

Analytic Methods for Tactical Air Warfare: Air campaign and High-Energy laser Propagation Analyses

5. FUNDING NUMBERS

DASW01-03-0915

6. AUTHOR(S)

David Lee, Robert Hemm, Scott Houser, John Dukovich, Jeremy Eckhause, Dou Long

7. PERFORMING ORGANIZATION NAME(S) AND ADDRESS(ES)

Logistics Management Institute
2000 Corporate Ridge
McLean, VA 22102-7805

8. PERFORMING ORGANIZATION REPORT NUMBER

LMI– PA304T1

9. SPONSORING/MONITORING AGENCY NAME(S) AND ADDRESS(ES)

Mr. Frank Lewis
OSD/Program Analysis and Evaluation - TACAIR
Pentagon, Rm 2C281
Washington, DC 20301-1800

10. SPONSORING/MONITORING AGENCY REPORT NUMBER

11. SUPPLEMENTARY NOTES

12a. DISTRIBUTION/AVAILABILITY STATEMENT

A Approved for public release; distribution is unlimited.

12b. DISTRIBUTION CODE

13. ABSTRACT (Maximum 200 words)

The report describes analytical tasks performed for OSD/PA&E TACAIR during the period from June 2003 through September 2004. The report describes a probabilistic model of campaigns for air superiority between two opponents, an analysis of force concentration in deterministic Lanchester campaigns, and an analysis of high-energy laser propagation. The campaign model is built on research conducted in previous tasks. The primary scenario has relatively few, technically superior defenders being attacked by numerous, technically inferior attackers. The model includes options for both attacker and defender force packages. The ability of the defender to identify and select high value attack formations is a selectable model option. In the model , the attacker optimizes its order-of-battle based on the expected values of targets destroyed and defenders killed. In addition to the model discussions, the report contains a mathematical derivation of force concentration benefits in deterministic Lanchester campaigns. Finally, the report describes a mathematical analysis of high-energy laser propagation for a 1.312 micron wavelength iodine laser, including diffraction, jitter, scattering, turbulence, and thermal blooming. The laser analysis is embodied in a spreadsheet model.

14. SUBJECT TERMS

Multiple air combat, campaign models, high-energy laser, propagation, Lanchester models

15. NUMBER OF PAGES

37

16. PRICE CODE

17. SECURITY CLASSIFICATION OF REPORT	18. SECURITY CLASSIFICATION OF THIS PAGE	19. SECURITY CLASSIFICATION OF ABSTRACT	20. LIMITATION OF ABSTRACT
Unclassified	Unclassified	Unclassified	UL

Contents

INTRODUCTION 1

AN APPLICATION OF A STOCHASTIC MODEL OF AN AIR SUPERIORITY CAMPAIGN 3

Scoring Air-to-Ground Success 3

Scoring of Aircraft 6

Campaigns and Their Results 6

ANALYSIS OF FORCE CONCENTRATION IN DETERMINISTIC LANCHESTER CAMPAIGNS 12

Background 12

Statement of the Problem 13

Results 13

Discussion 16

ANALYZING LASER WEAPONS FOR TACTICAL AIRCRAFT 17

Background 17

Overview 17

Extinction 17

Turbulence 18

Numerical Evaluation of Path Integrals 20

A Consistency Check Integral 23

Numerical Method 23

Results 24

Blooming 26

Stable Secondary Atmospheric Motions 31

SUMMARY AND CONCLUSIONS 33

REFERENCES 35

Figures

Figure 1. Model Structure 3

Figure 2. Bomber Value Delivered 7

Figure 3. Red Fighters Available 8

Figure 4. Red Bombers Available 8
Figure 5. Blue Fighters Available 8
Figure 6. Interception Statistics 9
Figure 7. Bomber Damage Value Comparison 10
Figure 8. Blue Aircraft Available Comparison 10
Figure 9. Red Aircraft Available 11
Figure 10. Verification of MLS Refractive Index Model 20
Figure 11. Verification of Derivative of MLS Refractive Index Model 21
Figure 12. Refracted and Straight Paths 22
Figure 13. Coordinate System 22
Figure 14. 1 kW/cm^2 Contours 24
Figure 15. Contour Detail 25
Figure 16. 0.1 kW/cm^2 Contour 25
Figure 17. Comparing Molecular Absorption 27
Figure 18. Extinction Coefficient Model and Data 27
Figure 19. Broadened, Wandering Spot 28
Figure 20. Atmospheric Waves, Made Visible by Clouds 32

Tables

Table 1. Aircraft Values as Bombers 5
Table 2. Day One Red Attack Packages 7
Table 3. CLEAR I Night Parameters 20

Air Campaign and High-Energy Laser Propagation Analyses

INTRODUCTION

This report covers work LMI did from July 2003 through September 2004 for the Tactical Air Forces Division of Program Analysis and Evaluation (PA&E TACAIR) in the Office of the Secretary of Defense. The purpose for this study and its predecessor studies was to develop tools for analyzing tactical air forces that meet three criteria;

- The time required to set the tools up and run them to generate usable information should be relatively short—minutes, not days. This criterion is important because analysts in PA&E TACAIR must deal with a great many hurried requests for substantial amounts of accurate information.

- The tools should operate on widely available personal computer (PC) platforms without highly specialized software. This criterion is important because the analysts should be able to use the tools in readily available environments without extensive training.

- The tools should account rationally and quantitatively for the uncertainties inherent in air combat. This criterion is important because PA&E TAC AIR advises the senior leadership of the Department of Defense, and these clients need quantitative measures of both central tendencies and dispersions to make good decisions.

To meet the three criteria, LMI researchers invested considerable effort in identifying the most salient features of the aspects of tactical air engagements that we treated and in constructing models that deal with them as effectively as possible under the limitations imposed by the first two criteria.

The report has three major sections. The first, "An Application of a Stochastic Model of an Air Superiority Campaign." discusses details of, and results from, the Stochastic Lanchester Air-to-Air Campaign Model (SLAACM). This section continues work previously reported by LMI [1 and 2].

The second section of the report, "Analysis of Force Concentrations in Deterministic Lanchester Campaigns," documents an analysis of conditions under which a weaker force can divide and overcome a stronger force.

The third section of the report, "Analyzing Laser Weapons for Tactical Aircraft," discusses the algorithms and data being used to analyze the potential performance of

tactical high energy lasers. It also discusses the progress of transforming these analyses into a spreadsheet-based Airborne Laser Infrared Transmission (ALIRT) model.

Other support efforts provided under this task, including a user's guide for the current version of SLAACM and a feasibility study for collection and analysis of Battle-of-Britain air engagement and campaign data are documented separately.

AN APPLICATION OF A STOCHASTIC MODEL OF AN AIR SUPERIORITY CAMPAIGN

This section describes an update of the campaign model described in *Stochastic Models of Air Superiority Engagements and Campaigns* [1] and gives an example application. The update accommodates impacts of varying air-to-ground weapon payload quantity and quality of the bomber types and the effect of the defenders' ability to identify the aircraft types making up an attack package. The application treats a campaign scenario in which an attacking force of many, relatively weak aircraft confronts a defending force of fewer, much stronger machines. In previous work, we analyzed individual engagements and the combination of engagements into a campaign. Below, we address evaluation of the air-to-ground campaign, considering optimal operations of both attacker and defender.

Scoring Air-to-Ground Success

We wish to score the value of an attack package to Red with a measure of the value of the targets that the package's payload is expected to destroy. First, let us consider how the value of a target may be expected to scale with the yield of a bomb required to destroy it.

VALUE AND LETHAL RADIUS AS FUNCTIONS OF YIELD

To see how value should vary as a function of the explosive yield required to destroy it, we considered the cost of hardening a target against a given yield. We then assume that the target's value is proportional to that cost.

To see how the yield required to destroy a structure varies with properties of the structure, we considered a simple model reinforcing structure, shown in Figure 1. The structure has depth (into the page) of w.

Figure 1. Model Structure

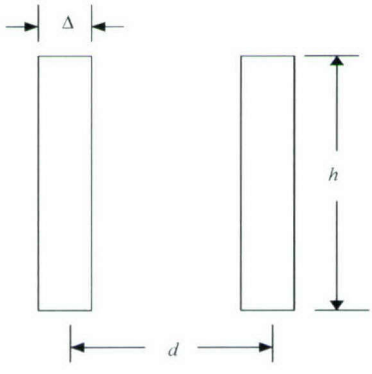

Pressure p on the structure's leftmost face will induce both axial and shear loads in the reinforcing columns. The axial load will be pwh^2/d, compressive on the rightmost column and tensile on the other. The shear loads on each column will be pwh/2. This leads to additional stress of maximum amplitude close to $ph^2/d\Delta$. If this stress is reacted by

material of maximum stress σ_{mx}, then the thickness Δ of the reinforcing columns must be $ph^2/d\,\sigma_{mx}$. We assume that the cost of reinforcement is proportional to the columns' volume. Thus we are led to the conclusion that the cost of hardening the structure against overpressure p is proportional to $pwh^3/\,d\,\sigma_{mx}$, for a given structure and reinforcing material—that is, for given w, h, d, and σ_{mx}— the cost of hardening is simply proportional to overpressure p.

We used dimensional analysis to see how pressure load varies with explosive yield E, assuming that the pressure is dynamic pressure induced by the air velocity v immediately behind the blast's shock wave. In addition to E, parameters for the blast wave are initial air density ρ_0 and the time. It follows that v is proportional to $(E/\,\rho_0)^{1/5}t^{-3/5}$. Since the radius of the blast wave increases monotonically with time, evaluating v at a given radius is equivalent to evaluating v at a given time. Thus the value of v at a given radius r is proportional to $E^{1/5}$, and the dynamic pressure $p \propto v^2 \propto E^{2/5}$. Thus we are led to take the cost of hardening a structure as proportional to the 2/5 power of the explosive yield against which the structure is hardened.

Dimensional analysis also lets us describe the variation of the lethal radius r_L of an explosion of yield E against a target hardened to withstand dynamic pressure p. If $r_L \propto E^a\,p^b$, then a = 1/3 and b = -1/3. That is, $r_L \propto (E/p)^{1/3}$.

Value of Targets Destroyed by a Given Payload

The single shot kill probability (sspk) that a target is destroyed in one attack by an explosion of lethal radius r_L when delivered by a system with a specified circular error probable (CEP) is

$$\text{sspk} = 1 - \left(\frac{1}{2}\right)^{r_L^2/\text{CEP}^2} \qquad \text{[Eq. 1]}$$

Recalling the variation of r_L with E and p, we see that if we refer r_L to some standard value r_{Lref}, hardness p to some standard value p_{ref}, and CEP to some standard value CEP_{ref}, then (1) and the fact that $r_L \propto (E/p)^{1/3}$ imply that

$$\text{sspk} = 1 - \left(\frac{1}{2}\right)^{\frac{r_{Lref}^2}{\text{CEP}_{ref}^2}\left(\frac{E}{E_{ref}}\frac{p_{ref}}{p}\right)^{2/3}\left(\frac{\text{CEP}_{ref}}{\text{CEP}}\right)^2} \qquad \text{[Eq. 2]}$$

Equation 2 gives us means of determining sspk for varying yield, hardness, and CEP. We will assume that a given aircraft and load combination will be sent against targets such that $r_{Lref} = \text{CEP}_{ref}$. We further assume that the yield is matched to the target, so that $E/E_{ref} = p_{ref}/p = 1$. Then

$$\text{sspk} = 1 - \left(\frac{1}{2}\right)^{\left(\frac{\text{CEP}_{ref}}{\text{CEP}}\right)^2} \qquad \text{[Eq. 3]}$$

If an aircraft with payload P carries bombs of weight 500w, where w is 1, 2, or 4, then the number of bombs carried is

$$N = \left\lfloor \frac{P}{500w} \right\rfloor \qquad \text{[Eq. 4]}$$

Note that the brackets that close only on the bottom indicate that the result is rounded down to the next lowest integer. This is called a "floor function" and is equivalent to a truncation function. Conversely, brackets closed only at the top designate a "ceiling function" where the result is rounded up to the next higher integer.

If each bomb carried is dropped on a different target, the expected number of kills is

$$< \text{targets killed} > = \left\lfloor \frac{P}{500w} \right\rfloor \left[1 - \left(\frac{1}{2} \right)^{\frac{CEP_{ref}^2}{CEP^2}} \right] \qquad \text{[Eq. 5]}$$

The value of the targets varies as the 2/5 power of the explosive yield required to destroy them. In view of this, the expected value of the targets killed, relative to some reference value, $value_{ref}$, is

$$< \frac{value}{value_{ref}} > = \left\lfloor \frac{P}{500w} \right\rfloor \left[1 - \left(\frac{1}{2} \right)^{\frac{CEP_{ref}^2}{CEP^2}} \right] \left(w^{2/5} \right) \qquad \text{[Eq. 6]}$$

We used Equation 6 to determine the values of bombers having various values of payload and CEP. Table 1 shows the results. For completeness, we included fighters, which could be used as bombers.

Table 1. Aircraft Values as Bombers

Aircraft	Weapon parameters			Weapon value versus:			Summary results	
	Payload	CEP	SSPK	500-lb target	1,000-lb target	2,000-lb target	Average value	Relative average value
RED_F1	1,000	1	0.50	1.0	0.7	0.0	0.6	1.0
RED_F2	1,000	1	0.50	1.0	0.7	0.0	0.6	1.0
RED_F3	2,000	1	0.50	2.0	1.3	0.9	1.4	3.0
RED_F4	3,000	0.6	0.85	5.1	3.4	2.2	3.6	6.0
RED_F5	6,000	0.1	1.00	12.0	7.9	5.2	8.4	15.0
RED_FB1	2,000	0.6	0.85	3.4	2.3	1.5	2.4	4.0
RED_B2	6,000	0.4	0.99	11.8	7.8	5.2	8.3	15.0
RED_B3	18,000	0.1	1.00	36.0	23.8	15.7	25.1	45.0

Scoring of Aircraft

Value to Red of a Blue Fighter Killed

Assuming Blue aircraft have 8 missiles, with sspk of 0.8, sending a single flight of 4 Blues against two, 12-aircraft attack packages gives less than 83 percent probability of killing all 24 opponents. Therefore, Blue is likely to use its aircraft in flights of 4 against only one attack package of 12 aircraft. In one mission, each Blue aircraft is, therefore, "worth" 3 Red aircraft. The average value of Red aircraft is roughly 6, and so we took the value to Red of killing a Blue aircraft to be 18.

With the scoring values thus developed, we took the Red payoff of an attack package to be four times the product of the probability that the bombers got past Blue defenders and the value of the individual bombers as shown in Table 1, plus 18 times the expected number of Blue aircraft killed.

We developed distributions of Red and Blue losses, and the probability that the bombers got through the defenders (that is, the probability that not all 8 escorts were killed), from the following variation of the classic stochastic Lanchester engagement model: first, the 4 advanced escorts engaged the Blue defenders in a 4-Vs-4 engagement to annihilation on both sides. Then, any surviving Blue aircraft engaged the 4 close-in escorts; again all engagements were to annihilation.[1]

Values for Blue

We assigned Blue's penalty for losing a Blue fighter as 40. We assigned Blue's benefit for killing a Red bomber as that bomber's value to Red.

Campaigns and Their Results

We modeled campaigns in the following way. Starting with the Red order of battle, we developed an optimal Red assault as the set of assault packages that maximized Red's expected payoff, subject to the constraints imposed by the numbers of aircraft of the various types available. An assault package is described by the ordered triple [advanced escort, close escort, bomber]. There are 45 possible package options, if Red uses only Red_FB1, Red_B2, and Red_B3 as bombers.

We modeled Blue's response in two ways: in the first, we assumed that Blue had perfect knowledge of the aircraft types making up each attack package. That enabled Blue to respond by attacking that set of Red attack packages that maximized Blue's expected payoff.

In the second, we assumed that Blue had no information about the aircraft in an attack package before attacking it. In this case, the Red attack packages are intercepted entirely at random.

[1] "Annihilation" here means that the combat runs until all the aircraft of one of the sides are destroyed.

The following sections show day-by-day results for the two cases of Blue's knowledge of the composition of Red's attack packages.

Results When Blue Has Adequate Battle Management and Perfect Knowledge of Red's Packages

We first treat a campaign in which Blue has perfect knowledge of the aircraft types in each attack package and has adequate battle management capability to assign the M available Blue flights to any M of the attack packages.

On the first day, Red's optimization led to the set of attack packages shown in Table 2.

Table 2. Day One Red Attack Packages

Number of packages	Advanced escort	Close escort	Bomber
29	Red_F5	Red_F5	Red_B3
2	Red_F5	Red_F5	Red_B2
6	Red_F4	Red_F4	Red_FB1
28	Red_F3	Red_F3	Red_FB1
50	Red_F2	Red_F2	Red_FB1
41	Red_F2	Red_F2	Red_B2
40	Red_F1	Red_F1	Red_F1
1	Red_F1	Red_F1	Red_B2

Blue's optimal response was to send all 25 available fighter flights against the most threatening attack packages, i.e., those with Red_F5 for both escorts and Red_B3 as the bomber.

We continued this campaign, taking expected values of the losses of all aircraft. Figures 2–5 show how it evolved.

Figure 2. Bomber Value Delivered

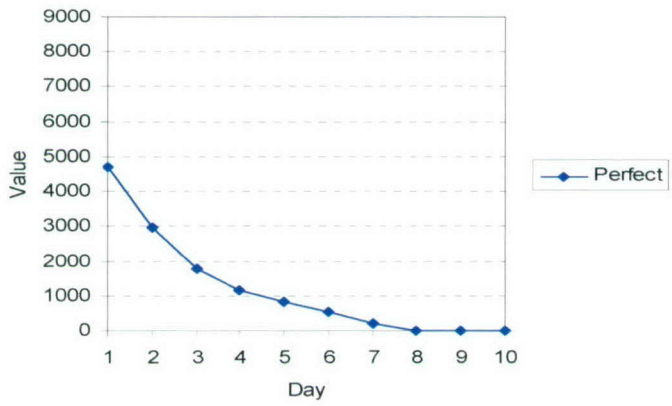

By "Bomber Value Delivered," we mean the total expected destructive value of the bombers not killed by Blue defenders, either because their flights were not intercepted (the most common cause) or because their package's escorts destroyed all four Blue defenders.

Figure 3. Red Fighters Available

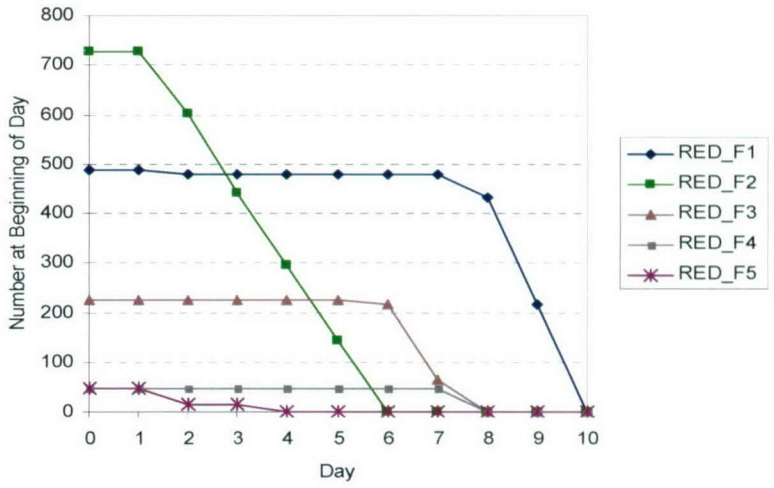

Figure 4. Red Bombers Available

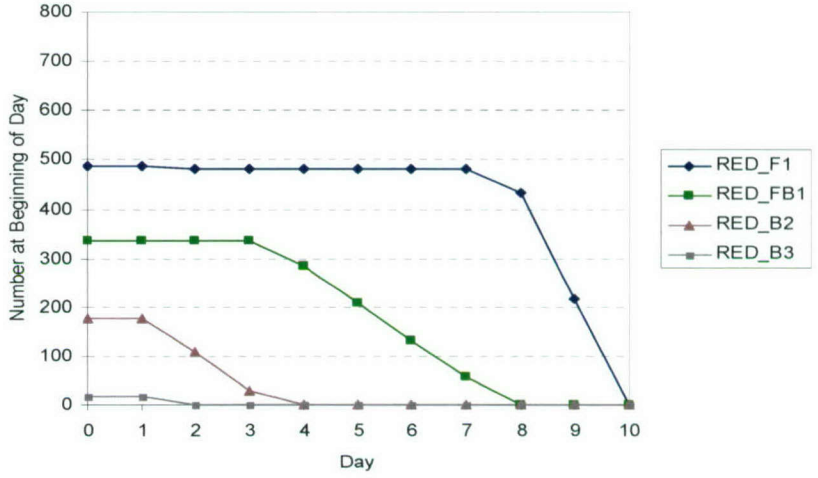

Figure 5. Blue Fighters Available

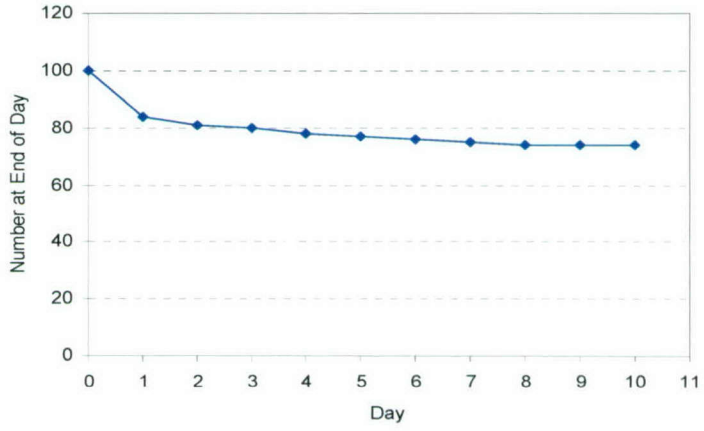

Results When Blue Encounters Red Packages at Random

For random interceptions, if there are J distinct types of attack packages, with N_j packages of type j, and a total of $N \equiv \sum_{j=1}^{J} N_j$ attack packages launched in the Red assault, and M defending flights respond, then the probability $P(n_1, n_2, \ldots, n_J)$ that n_1 packages of type 1, n_2 packages of type 2, …, n_J packages of type J are intercepted is

$$P(n_1, n_2, \ldots, n_J) = \frac{M!}{\prod_{i=1}^{J} n_i!} \frac{(N-M)!}{N!} \prod_{j=1}^{J} \frac{N_j!}{(N_j - n_j)!} \qquad \text{[Eq. 7]}$$

The distribution of the attack packages intercepted when Blue intercepts them entirely at random is dispersed, in the sense that many distinct sets of intercepted packages, characterized by the n_i of Equation 7, have nearly the same probability. The impact of this dispersion may be mitigated, however, by the fact that the sets of packages that are intercepted with relatively high probability all have nearly the same bomber-damage value and blue losses. Figure 6 illustrates this, showing probability, expected bomber-damage value, and expected total Blue losses for the 12 most likely interceptions.

Figure 6. Interception Statistics

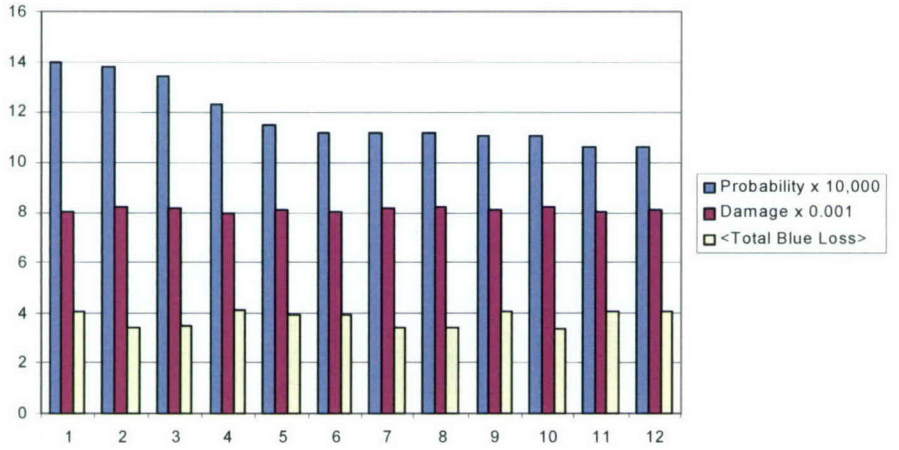

To determine damage, and the next day's Blue force, we assumed that the mode of the Equation 7 distribution occurred. In all the cases that we considered, the mode did not differ significantly from the mean, rounded to integer values.

Figures 7 and 8 compare damage value and Blue aircraft available for the first two days of the "perfect information" and "random intercept" campaigns. Figure 7 shows the substantial value of Blue being able to put its assets against only the most threatening attack packages. The total damage values are 34,100 units for

the "random" case and 12,152 damage units for the "perfect" case. Perfect knowledge, thus, results in a 64 percent reduction in enemy damage.[2]

Figure 7. Bomber Damage Value Comparison

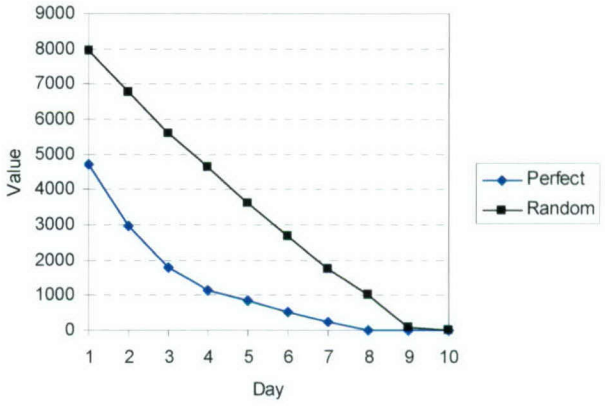

Figure 8 shows that Blue's initial losses will be less in the "random" case, because Blue does not fight as many engagements with Red's best fighters as in the "perfect" case. We see here that, in order to achieve the dramatic reduction in Red damage with perfect knowledge, Blue must not flinch in the face of severe initial losses.

Figure 8. Blue Aircraft Available Comparison

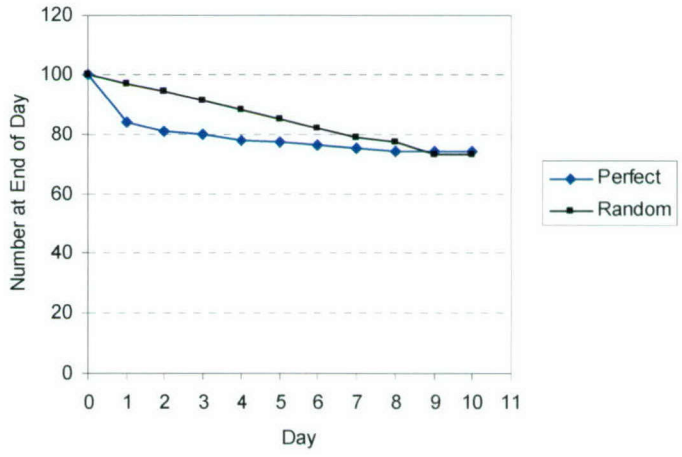

[2] The corresponding values in tons of bombs dropped are 7,076 for the random case and 2,768 for the perfect case, resulting in a 61 percent reduction due to perfect knowledge.

Figure 9 shows the variation of the numbers of the various types of Red aircraft.

Figure 9. Red Aircraft Available

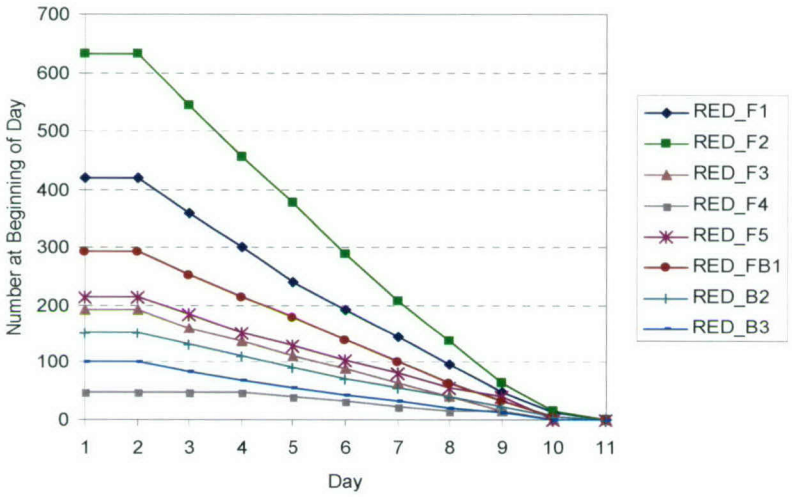

Figure 9 shows consistent, linear decreases in the numbers of each type of Red aircraft. This contrasts sharply with the variations shown in Figures 3 and 4. For the campaign described in those figures, Blue's perfect information about the composition of Red packages allows Blue to concentrate systematically on the most threatening formations. With the random interceptions, and the great dominance of Blue's aircraft, the rate of decrease of a Red aircraft type will be roughly proportional to the fraction of the total number of Reds that the type represents. Those fractions are roughly constant through the campaign's first 4 days.

Analysis of Force Concentration in Deterministic Lanchester Campaigns

In this section we show that, in the context of the force-on-force Lanchester model, the smallest number of engagements with which an inferior force can annihilate a stronger one by repeated force concentration is $\left\lceil \frac{1}{\rho_0} \right\rceil$, where ρ_0 is the initial force ratio. We also derive some optimal force-concentration strategies.

Background

The analysis of force concentration is a major theme of Lanchester's seminal paper [3]. Subsequent work has extended Lanchester's results, for example, by considering optimal allocations of elements of a superior force [4].

In the context of the Lanchester force-on-force model, which is defined in Taylor [5], a weaker force can defeat a stronger one by force concentration in a series of engagements. Lanchester [3] cites Nelson's plan for the battle of Trafalgar as an example. The British fleet was weaker than the French-Spanish combined fleet that they faced, by a force ratio of about 3:4. In his plan, Nelson concentrated essentially all his force on half the enemy forces. The British would have had a roughly 2–1 force-ratio advantage in this initial engagement, which they would have won with sufficient survivors to defeat the other half of the enemy force. Thus Nelson's plan would have been expected to result in victory in a sequence of two engagements.

This suggests the possibility of a general strategy for a weaker force to annihilate a stronger one, by successively concentrating all available force on selected fractions of the enemy force. Let us call the weaker force Red, the stronger, Blue. Perhaps if Red concentrates all its force on a fraction f_0 of the Blue force, Red can win that engagement and also a subsequent engagement between the survivors. If so, Red will win the campaign in two engagements. If that is not possible, perhaps by concentrating all its forces on a fraction f_0 of the Blue force, and then concentrating the surviving Red force on a fraction f_1 of the surviving Blue force, Red can, in a third engagement, annihilate all the Blues who survive the second engagement, and so win the campaign in three engagements. If that is not possible, perhaps in a similar way Red can win in four engagements, or, if not in four, perhaps in five, and so on.

The purpose of this analysis is to examine this strategy in general. We will exhibit a lower bound on the number of such engagements and derive some optimal strategies.

Statement of the Problem

A Red force with R_0 units of effectiveness k_r confronts a Blue force with B_0 elements of effectiveness k_b. The Red force is weaker, in the sense that force ratio ρ_0 of these initial forces,

$$\rho_0 = \frac{k_r R_0^2}{k_b B_0^2} \qquad \text{[Eq. 8]}$$

is less than one.[3] Thus Red will lose an engagement with the entire Blue force. But perhaps if Red concentrates all his force on a fraction f_0 of the Blue force, he can win that engagement and also a subsequent engagement between the Red and Blue forces that survive it. If so, Red will win the campaign in two engagements. If that is not possible, perhaps by concentrating all his forces on a fraction f_0 of the Blue force, and then concentrating his surviving force on a fraction f_1 of the surviving Blue force, Red can, in a third engagement, annihilate all the Blues who survive the second engagement, and so win the campaign in three engagements.

The problem we consider is to determine the smallest number of engagements with which Red can, by concentrating its force on specified fractions f_0, f_1, ... of the Blue force confronting him, annihilate the Blue force. We also wish to determine choices of sequences f_0, f_1, ... that minimize Red's losses.

Results

Our principal results can be stated conveniently as two theorems:

1. Theorem 1. A necessary and sufficient condition that Red can win the campaign in as few as N engagements, N = 2, 3, ..., is that $\rho_0 > 1/N$.

2. Theorem 2. If Red wins the campaign in N engagements, the sequence f_0, f_1, ..., f_{N-2} that minimizes Red's losses is

$$f_i = \frac{1}{N-i}, \quad i = 0,1,\ldots,(N-2) \qquad \text{[Eq. 9]}$$

and R_N^2, the square of the number of surviving Reds, is given by

$$R_N^2 = R_0^2 - \frac{k_b B_0^2}{k_r} J_N^* \qquad \text{[Eq. 10]}$$

[3] $k_x X^2$ is also referred to as the fighting strength of the forces, and ρ_0 referred to as the strength ratio.

where $J_N^* = 1/N$.

Two lemmas facilitate proofs of the theorems:

1. Lemma 1. The function $g_N(x)$,

$$g_N(x) \equiv \frac{1}{N}(1-x)^2 + x^2 \qquad \text{[Eq. 11]}$$

has a unique minimum at $x = 1/(N + 1)$.

Proof: $g'_N(x)$ is continuous, negative for $x < 1/(N+1)$ and positive for $x > 1/(N+1)$.

It will also be useful to note that $g_N(1/(N + 1)) = 1/(N + 1)$.

2. Lemma 2. A necessary and sufficient condition that there are values of f in (0,1) such that

$$\frac{\rho - f^2}{(1-f)^2} > \frac{1}{N} \qquad \text{[Eq. 12]}$$

is that $\rho > 1/(N + 1)$, for integer $N \geq 2$.

Proof: Inequality 12 implies

$$\rho > \frac{1}{N}(1-f)^2 + f^2 \equiv g_N(f) \qquad \text{[Eq. 13]}$$

Necessity then follows from Lemma 1. By the continuity of $g_N(x)$, if $\rho > 1/(N+1)$ there is a neighborhood of $f = 1/(N+1)$ for which Equation 13, and consequently Inequality 12, is satisfied. Since $0 < 1/(N + 1) < 1$ for $N \geq 2$, there is also a sub-interval of (0,1) within which Inequality 12 is met, and that establishes sufficiency.

PROOF OF THEOREM 1: We proceed by induction on N. Let N = 2. For Red to win the first engagement,

$$\frac{k_r R_0^2}{k_b B_0^2 f_0^2} = \frac{\rho_0}{f_0^2} > 1 \qquad \text{[Eq. 14]}$$

When Inequality 14 is satisfied, the second engagement will have force ratio ρ_1 given by

$$\rho_1 = \frac{R_0^2 - k_b B_0^2 f_0^2}{(1-f_0)^2} = \frac{\rho_0 - f_0^2}{(1-f_0)^2} \qquad \text{[Eq. 15]}$$

Thus Red will annihilate the Blue force in two engagements if and only if (iff) $\rho_1 > 1$ and Inequality 14 is met. But Inequality 14 is satisfied for all $f_0 \in (0, 1)$ that make $\rho_1 > 1$, since

$$\frac{\rho_0 - f_0^2}{(1-f_0)^2} > 1 \Rightarrow \rho_0 > (1-f_0)^2 + f_0^2 \Rightarrow \frac{\rho_0}{f_0^2} > \frac{(1-f_0)^2}{f_0^2} + 1 \qquad \text{[Eq. 16]}$$

By Lemma 2, there are such values of f_0 iff $\rho_0 > 1/2$, so the theorem's statement is correct for $N = 2$.

Now suppose the statement is correct for $N = K$. Then Red can win in $K + 1$ engagements if (6) is met, and if it is possible to choose f_0 such that $\rho_1 > 1/K$. By (8) and Lemma 2, this is possible iff $\rho_0 > 1/(K + 1)$, which completes the induction.

- Corollary to Theorem 1: The smallest number N of engagements with which an inferior force can annihilate a superior one by force concentration in successive engagements is $\left\lceil \frac{1}{\rho_0} \right\rceil$.

PROOF OF THEOREM 2: Again we proceed by induction. First, we note that when Red annihilates the Blue force in a sequence of N engagements, the number R_N of surviving Red elements is given by

$$\begin{aligned} R_N^2 = R_0^2 - \frac{k_b B_0^2}{k_r}\Big[& f_0^2 + (1-f_0)^2 f_1^2 - (1-f_0)^2(1-f_1)^2 f_2^2 + .. \\ & + (1-f_0)^2(1-f_1)^2 ... (1-f_{N-3})^2 f_{N-2}^2 \\ & + (1-f_0)^2(1-f_1)^2 ... (1-f_{N-3})^2 (1-f_{N-2})^2 \Big] \end{aligned} \qquad \text{[Eq. 17]}$$

Thus the number of Red survivors will be maximized by the choice $f_0, f_1, \ldots, f_{N-2}$ that minimizes J_N, where

$$\begin{aligned} J_N(f_0, f_1, ..., f_{N-2}) \equiv \Big[& f_0^2 + (1-f_0)^2 f_1^2 + (1-f_0)^2(1-f_1)^2 f_2^2 + .. \\ & + (1-f_0)^2(1-f_1)^2 ... (1-f_{N-3})^2 f_{N-2}^2 \\ & + (1-f_0)^2(1-f_1)^2 ... (1-f_{N-3})^2 (1-f_{N-2})^2 \Big] \end{aligned} \qquad \text{[Eq. 18]}$$

Note that Equation 18 implies a recursion of the J_K,

$$J_{K+1}(f_0, f_1, ..., f_{K-1}) = f_0^2 + (1-f_0)^2 J_K(f_1, f_2, ..., f_{K-1}) \qquad \text{[Eq. 19]}$$

If $N = 2$, then $J_2(f_0) = g_1(f_0)$ and, by Lemma 1, the minimizing value of f_0 is 1/2, and J_2^*, the minimum value of J_2, is 1/2. Therefore the statement of Theorem 2 is correct for $N = 2$.

Now suppose the statement is correct for $N = K$. That is, suppose $J_K(f_0, f_1, \ldots, f_{K-2})$ is minimized by $f_j = 1/(K - j)$, $j = 0, 1, 2, \ldots, K - 2$, and that J_K^*, the smallest value of J_K, is given by $J_K^* = 1/K$.

Referring to Equation 19, we see that the coefficient of $J_K(f_1, f_2, \ldots, f_{K-1})$ is positive for all f_0, so J_{K+1} will be minimized by choosing $f_1, f_2, \ldots, f_{K-1}$ to minimize $J_K(f_1, f_2, \ldots, f_{K-1})$, and then choosing f_0 to minimize $f_0^2 + (1 - f_0)^2 J_K^*$, where J_K^* denotes the minimum value of J_K. By the hypothesis that the statement is true for $N = K$, we have $f_j = 1/(K + 1 - j)$, $j = 1, 2, \ldots, K - 1$. Also by that hypothesis, $J_K^* = 1/K$. Then, by Equation 19, f_0 must be chosen to minimize $g_K(f_0)$. By Lemma 1, that implies that $f_0 = 1/(K + 1)$, and that $J_{K+1}^* = 1/(K+1)$, which completes the induction.

Discussion

We believe the results reveal an interesting feature of the Lanchester force-on-force model. We also believe that the results are useful, not necessarily because commanders may apply them directly, as Admiral Nelson apparently did at Trafalgar, but rather, because it will prove useful to consider actual force concentration strategies in the light of knowledge of the limits on force concentration, and of optimal concentration strategies.

Lanchester [3] points out that dividing an opposing force into two equal segments gives the lowest possible total force. This is, of course, an example of Lemma 1 for $N = 1$.

While this report was in preparation, we learned of a paper by David Bitters[4], which obtains the principal result by another method.

[4] David Bitters, "Efficient Concentration of Forces, or How to Fight Outnumbered and Win," *Naval Research Logistics* **42**, pp. 397-418 (1995).

ANALYZING LASER WEAPONS FOR TACTICAL AIRCRAFT

Background

There is continuing interest in the potential for use of airborne, tactical, high energy laser weapons. Early efforts in this area focused on 10.6 micron (μ) wavelength carbon dioxide (CO_2) and 3.8 μ deuterium fluoride (DF) chemical lasers. Current interest is focused on 1.3 μ chemical oxygen iodine (COIL), and electrically-powered solid state lasers. The most mature solid state laser technology flashlamp-pumped 1.06 μ neodymium/yttrium aluminum garnet (Nd:YAG), however, diode pumping, and alternative lasing elements and substrates are under active consideration.[5]

Practical tactical laser weapons are conceded to be far in the future, but it is not too early to investigate potential laser performance and weapon utility. During this year we investigated the propagation properties of the iodine laser in the tactical environment. Future studies will include similar propagation studies of solid state lasers and engineering investigation of both COIL and solid state lasers.

Overview

In this section we describe a MSExcel workbook implementation of a method for calculating the peak fluence delivered to an airborne or ground-based target from a laser weapon on an airborne platform, when the beam propagates through the inhomogeneous, absorbing, scattering atmosphere (refraction and extinction) which is in turbulent motion (turbulence), and when heating of the air by the beam (blooming) may have significant effects. Results reported here are for one laser wavelength, that of the Chemical Oxygen-Iodine Laser (COIL), 1.3152 microns. Extending our methods to other, single-line wavelengths is straightforward.

The paragraphs below describe our methods for calculating the effects of atmospheric refraction, extinction, turbulence, and blooming on laser weapons for tactical aircraft. Its following four sections give details of our treatments of these effects.

Extinction

Our basic source of extinction information was PcLnWin, a graphical interface to the FASCODE atmospheric code provided by the Ontar Corporation.[6] PcLnWin is fully documented in such Ontar publications as *PcLnWin Manual, Version 3*, October 1999.

[5] Solid state lasers typically include a lasing element such as neodymium dispersed in a host structural material such as yttrium aluminum garnet.

[6] Ontar Corporation, 9 Village Way, North Andover, Massachusetts 01845.

PcLnWin/FASCODE requires certain user inputs, while providing default values for many FASCODE inputs. The user inputs that we used were

- *Line file*. Using data provided with PcLnWin, we built a line file covering the wavenumber interval from 7224.491 cm^{-1} to 7983.610 cm^{-1}, roughly ±5 percent from the COIL wavenumber of 7604.523 cm^{-1}. The file includes N_2, O_2, H_2O, CO_2, O_3, N_2O, CO, and CH_4 molecules.

- *Atmosphere*. We developed results for three of PcLnWin's available atmosphere models: the 1976 U. S. Standard Atmosphere, and two models assembled by Ontar from various sources to treat the winter atmosphere in midlatitudes, and the summer atmosphere in mid latitudes. We will refer to these three atmosphere models as Std, MLW, and MLS, respectively.

- *Aerosol*. We chose FASCODE's Rural aerosol. This choice gives 23 km visibility at the surface.

- *Troposphere/Stratosphere*. This transition was determined by the atmosphere model used.

- *Geometry*. For our initial calculations, we used the PcLnWin option of specifying observer height, final height, and earth-centered angle. In several cases we verified that the refracted path that we computed (our computations are described below in the section "Path Integrals") agreed with the one computed by FASCODE. Later, as described under "Blooming," we developed analytic models of the altitude variations of aerosol absorption and scattering, and of molecular absorption, to treat STD, MLW and MLS atmospheres. We also developed analytic models of the altitude variation of refractive index for the MLW and MLS atmospheres. The STD atmosphere's refractive index variation is analytic, as described below under "Numerical Evaluation of Path Integrals."

Turbulence

Our principal parameter for turbulence effects is the Strehl ratio SR,

$$SR \equiv \frac{\text{Maximum fluence with turbulence}}{\text{Maximum fluence in diffraction limit}} = \frac{4}{\pi}\left(\frac{D}{\lambda L}\right)^2 \frac{1}{P}(\text{Maximum fluence with turbulence}) \quad \text{[Eq. 20]}$$

In Equation 20, D is the diameter of the laser's telescope's mirror, and λ is the wavelength of the radiation. L is the length of the laser-to-target path undisturbed by turbulence, and P is the laser's power.

We used the expression for SR given by Sasiela in Equation 8.13, on page 164 of [6]:

$$SR = \frac{24}{5\sqrt{\pi}} \sum_{n=0}^{\infty} \frac{(-1)^n}{n!} \frac{\Gamma(3/2 + 5n/6)\,\Gamma(n+6/5)}{\Gamma(3+5n/6)\,\Gamma(n+11/5)} \left[3.44 \left(\frac{D}{r_0} \right)^{5/3} \right]^n \quad \text{[Eq. 21]}$$

We also used the asymptotic expansion for large values of r_0/D given in Sasiela's Equation 8.15.

The parameter r_0 is the coherence diameter imposed by turbulence, that is, the distance perpendicular to the propagation direction over which turbulent perturbations in refractive index allow coherence in the electromagnetic wave from the laser. We used Sasiela's expression for the coherence diameter of a spherical wave with focus at the target,

$$r_{0s} = \left(0.423\ k_0^2\ \mu_{5/3} \right)^{-3/5} \quad \text{[Eq. 22]}$$

Following Sasiela's Equation 4.6, we evaluated $\mu_{5/3}$ as the path integral

$$\mu_{5/3} = \int_0^L C_n^2(z)(L-z)^{5/3}\,dz \quad \text{[Eq. 23]}$$

where C_n^2 denotes the refractive index structure parameter of the turbulence.

C_n^2 varies with height, geographic location, time of day, and season. For cases involving propagation to the ground, we used the Hufnagel-Valley model for C_n^2,

$$C_n^2 = 8.2\times10^{-26} W^2 h^{10} e^{-h/1.0} + 2.7\times10^{-16} e^{-h/1.5} + A e^{-h/0.1} \quad \text{[Eq. 24]}$$

The expression of Equation 24 gives C_n^2 in $m^{-2/3}$ for h in km, W in m/sec, and A in $m^{-2/3}$. We used W = 21 m/sec and A = 1.7×10^{-14} $m^{-2/3}$. With this choice of parameters, the Hufnagel-Valley model is called the Hufnagel-Valley 5/7 model, because for vertical propagation downward through the entire atmosphere it gives, in standard models, a coherence radius of 5 cm and an isoplanatic angle of 7 microradians, for 0.5 micron radiation.

In some cases of air-to-air engagement, we modeled C_n^2 as 2×CLEAR I Night. This model is

$$\log_{10} C_n^2 = A + Bz + Cz^2 + D\exp\left[\{-0.5(z-E)/F\}^2\right]$$

where parameters A, B, C, D, E, and F are given in Table 3.

Table 3. CLEAR I Night Parameters

z	A	B	C	D	E	F
$1.23 < z \leq 2.13$	-10.7025	-4.3507	0.8141	0	NA	NA
$2.13 < z \leq 10.34$	-16.2897	0.0335	-0.0134	0	NA	NA
$10.34 < z \leq 30$	-17.0577	-0.0449	-0.0005	0.6181	15.5617	3.4666

Numerical Evaluation of Path Integrals

We evaluated the path integral in Equation 23, and certain other path integrals, numerically. To do so, we needed to compute the path taken by the laser's output through the atmosphere undisturbed by turbulence.

Effects of oxygen and nitrogen molecules dominate the atmosphere's refractive index. Following the expression for n given by Thomas and Duncan [7], we used

$$n = 0.079P / T \qquad \text{[Eq. 25]}$$

where P is pressure in atmospheres and T is temperature in ^{o}K.

For MLS and MLW atmospheres, we used analytic models of PcLnWin refractive index outputs. Calculation of the refracted ray requires derivatives of refractive index variation with height, so a continuously differentiable model is desirable. We made the models by linear interpolation in the divided differences of refractive index parameter, and integrated the resulting piecewise linear, continuous function with an added, adjustable constant of integration to obtain a continuously differentiable model of refractive index.

Figure 10 shows the comparison between our model of the refractive index parameter $1e^{6}(n - 1)$, where n is refractive index, and the PcLnWin data for MLS.

Figure 10. Verification of MLS Refractive Index Model

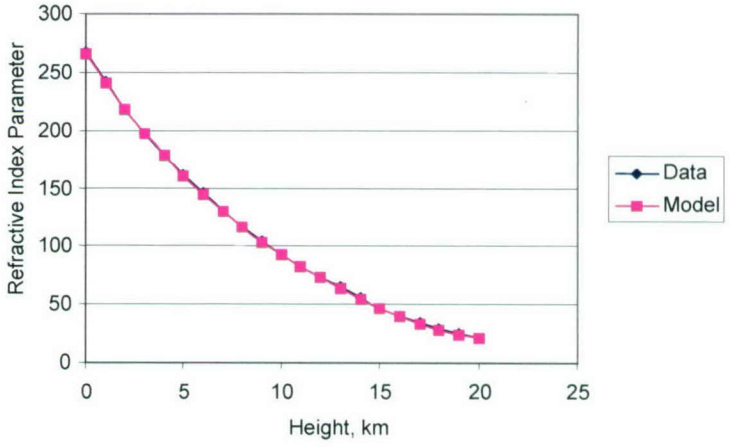

Figure 10 shows the comparison between divided differences of the refractive index parameter, and the derivative of our model of the refractive index parameter for MLS. The tropopause is clearly noticeable in Figure 11.

Figure 11. Verification of Derivative of MLS Refractive Index Model

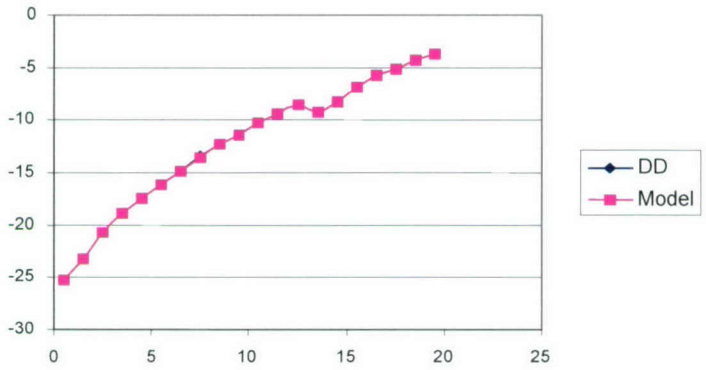

The refractive index variation of Thomas and Duncan [6] is not large; it is about 0.0003 near the surface. Also, tactical laser weapons will be used at medium ranges, generally no greater than 100–200 km. It is possible that using straight paths would not greatly distort integrals like that of Equation 23.

Two considerations militate against neglecting refraction, however. First, refraction is noticeable at extreme ranges and low weapon altitudes (

Figure 12). Second, and deciding, C_n^2 varies sharply with height, so that path variations may have significant effects. For example, C_n^2 differs by more than 10 percent on substantial parts of the two paths shown in

Figure 12 (please note that the great difference between the scales of the ordinate and abscissa of that figure distorts geometry).

Figure 12. Refracted and Straight Paths

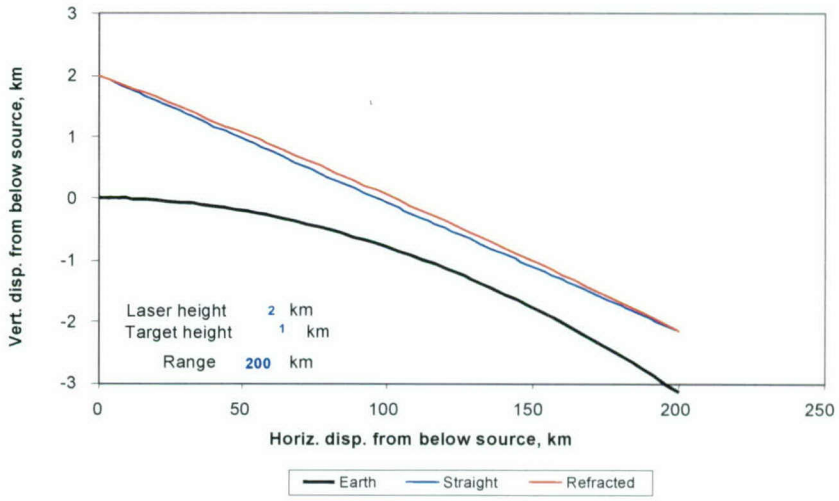

Accordingly, we determined refracted paths numerically. We did so by determining the path of minimum propagation time from weapon to target. We used the coordinate system shown in Figure 13

Figure 13. Coordinate System

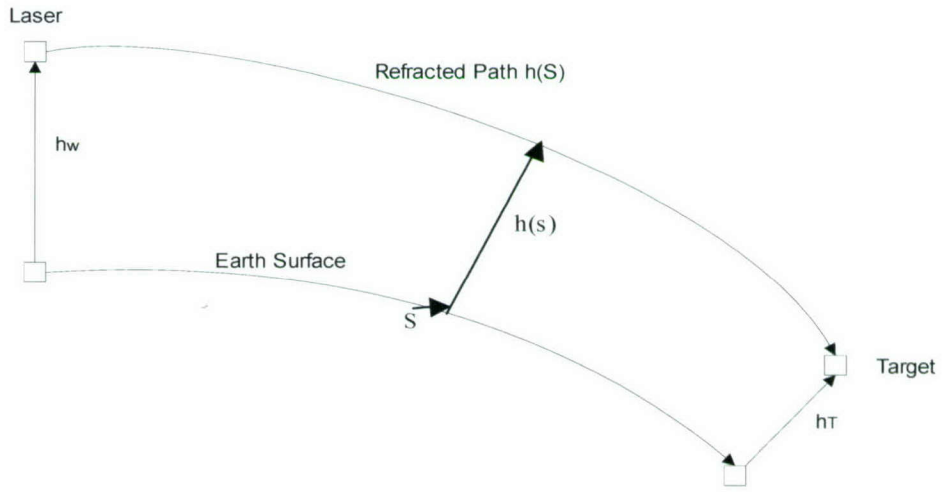

Specifically, the variational problem is

$$\min_{h(S)} \int_{S=0}^{S_L} \frac{\sqrt{(h')^2 + (1+h/R)^2}\,dS}{C(h(S))} \qquad \text{[Eq. 26]}$$

where R is the earth's radius and C is the speed of light. The familiar condition for the minimizing h(s),

$$\frac{\partial f}{\partial h} - \frac{d}{dS}\frac{\partial f}{\partial h'} = 0$$

where f(S,h,h′) is the integrand of Equation 26, leads to the system

$$h' = \frac{v(S)\,C\,(1 + h(S)/R)}{\sqrt{1 - v^2 C^2}}$$

$$v' = \frac{\sqrt{1 - v^2 C^2}}{RC} - \frac{1 + h/R}{\sqrt{1 - v^2 C^2}}\frac{1}{C^2}\frac{\partial C}{\partial h} \qquad \text{[Eq. 27]}$$

of ordinary differential equations. This system, with the boundary conditions

$$h(0) = h_W,\ h(S_L) = h_T \qquad \text{[Eq. 28]}$$

determines h(s).

A Consistency Check Integral

Our model for the Strehl ratio rests on the method of smooth perturbations (MSP) for treating the nonlinear Riccati equation for the logarithm of a field component, that arises in Rytov's method for determining the effects of turbulence. Sasiela [5] Section 2.2, pp. 30 et seq., notes that a necessary condition for the consistency of this method is

$$k_0^{7/6} \int_0^L C_n^2(h(z))(L - z)^{5/6}\,dz < 1$$

We evaluated this integral numerically to check on the consistency of the MSP.

Numerical Method

We determined contours of constant fluence, accounting for atmospheric extinction and turbulence, in this way: for a given value of desired fluence I_d, and for fixed laser height h_W and target height h_T, we varied earth-surface distance S to find values S1 and S2 that bracketed the value of S that made

$$I_{diff} \times \text{Strehl}(h_W, h_T, S) \times T(h_W, h_T, S) = I_d,$$

where $T(h_W, h_T, S)$ was calculated by PcLnWin, and where

$$I_{diff} \equiv \frac{\pi}{4}\left(\frac{D}{\lambda L}\right)^2 P$$

Specifically, we found S1 and S2 such that

$$I_{diff} \times Strehl(h_W, h_T, S1) \times T(h_W, h_T, S1) < I_d$$

and

$$I_{diff} \times Strehl(h_W, h_T, S2) \times T(h_W, h_T, S2) > I_d$$

By continuity, the desired value of S lies between S1 and S2, and we determined it by bisection. To avoid repeated calculations with PcLnWin, we used linear interpolation for transmissivity T, after S1 and S2 became sufficiently close. After bisection converged, we compared the exact value of T for the converged value of S, with the value from the linear interpolation and found, typically, 3- to 4-figure agreement. In later work, we used the analytic models of PcLnWin's extinction to determine that effect.

Results

The leftmost curve of Figure 14 shows the resulting contour of 1 kw/cm^2 peak fluence for the laser described in [11]. That laser has a power of 3 MW, and a mirror diameter of 1.5 m.

The rightmost contour shows the diffraction limit. It is a circle of radius 554 km, centered on the weapon. Please note that, to show details of vertical structure, the chart greatly expands the scale of the ordinate axis relative to that of the abscissa. This makes the circle appear straight and distorts other geometric relations. This contour's lowest point is at a height of 2 km, the lowest point for which the refracted ray from the source does not intersect the earth.

Figure 14. 1 kW/cm^2 Contours

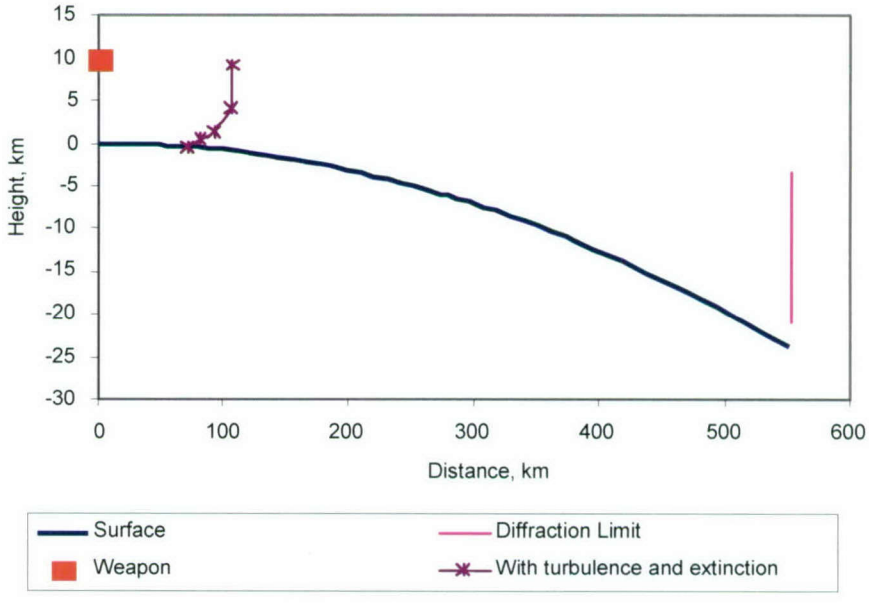

Figure 15 shows the 1kw/cm^2 contour in more detail. This figure suggests that, even without benefit of adaptive optics, the laser described in the APS article could deliver damaging fluence to a target despite the impacts of atmospheric extinction and turbulence, at tactically useful ranges.

Nevertheless, the degree to which such a laser would be useful as a tactical weapon still would depend on effects of blooming (which we consider in the next subsection) and on target orientation, geometry, albedo, and motion (which we do not consider in this report). Jitter in the airborne laser may also degrade performance; we consider this briefly below.

Figure 15. Contour Detail

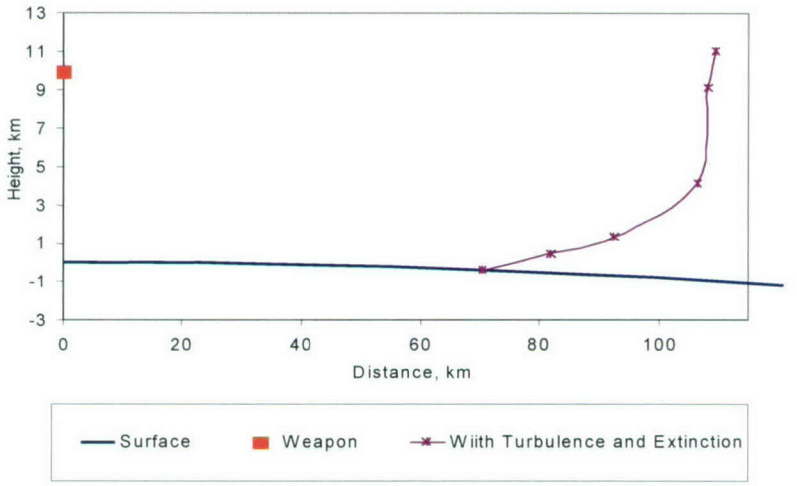

For insight into the variation of the range of a laser weapon without adaptive optics, Figure 16 shows the contour of 0.1 kw/cm^2 intensity.

Figure 16. 0.1 kW/cm^2 Contour

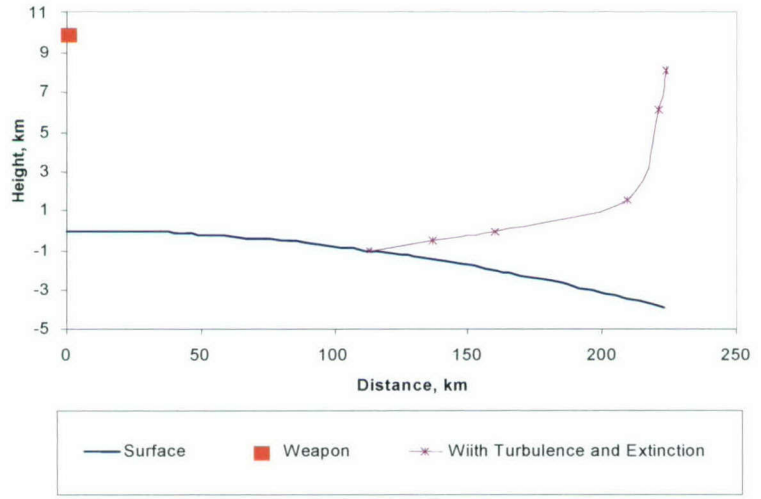

Blooming

The beam heats the air through which it passes, decreasing refractive index unevenly and distorting the beam. This effect, called "blooming," reduces fluence on the target. Here we consider this effect.

Citing an article by Weichel [8], the APS report says that, for a Gaussian beam having an e-folding radius a(z) where z is path length, the ratio of the intensity at the target with blooming to that without blooming is

$$\frac{\mathrm{I(Bloom)}}{\mathrm{I(NoBloom)}} = \frac{1}{1+(B_0 I_B)^2} \qquad \text{[Eq. 29]}$$

where

$$B_0 = -\frac{dn_0}{dT}\frac{\alpha_0 P L^2}{4\pi\rho_0 w_0 a_0^3} \qquad \text{[Eq. 30]}$$

and

$$I_B = \frac{2}{L^2}\int_{z=0}^{L}\frac{a_0}{a(z)}\left[\int_{z'=0}^{z}\frac{a_0^2 w_0 \alpha(z')T_0}{a^2(z')w(z')\alpha_0 T(z')}dz'\right]dz \qquad \text{[Eq. 31]}$$

In Equations 30 and 31, $\alpha(z)$ denotes the part of the atmospheric extinction coefficient that puts power into the air through which the beam passes, w(z) the effective wind velocity coming from the motion of the beam relative to the (possibly moving) atmosphere, T(z) the temperature, and a(z) the beam radius, all varying with distance z along the path. The subscript 0 on any of these denotes the corresponding value at z = 0.

The following subsections explain how we evaluated normalized extinction coefficient $\frac{\alpha(z)}{\alpha_0}$, beam radius $\frac{a(z)}{a_0}$, and wind profile $\frac{w(z)}{w_0}$.

Extinction and Absorption Coefficients

Using PcLnWin outputs, we developed analytic models of the variations of molecular absorption and atmospheric extinction coefficients with height.

Figure 17 compares our model of molecular absorption with the one used by Walter and Mani [9].

Figure 17. Comparing Molecular Absorption

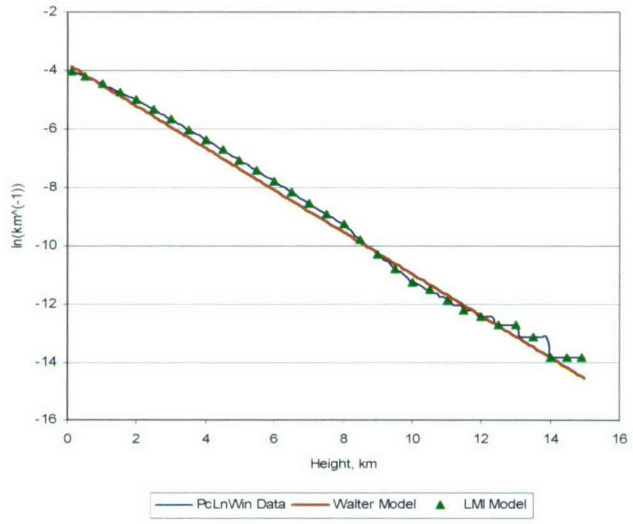

Figure 18 compares our extinction coefficient with the one used by Walter and Mani [9].

Figure 18. Extinction Coefficient Model and Data

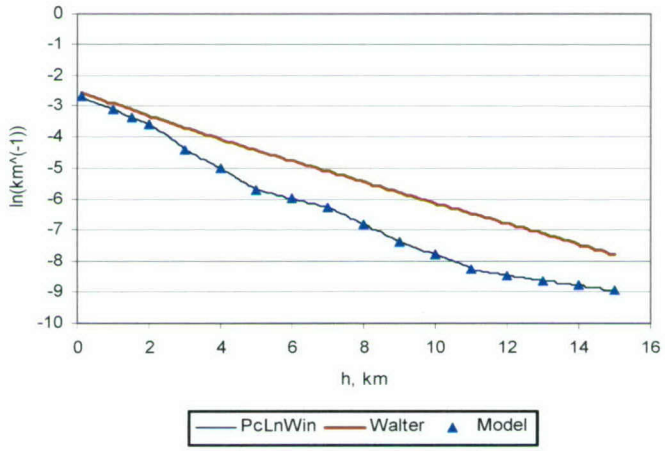

Figures 17 and 18 show that, while PcLnWin's molecular absorption agrees closely with Walter's results, PcLnWin's total extinction, and thus by implication aerosol absorption and extinction, are considerably larger for heights of 2 to 5 km than those of the model used by Walter and Mani.

BEAM RADIUS

For the variation of beam radius a(z), we assumed linear variation from the mirror radius at z = 0 to the radius of the turbulence-broadened, focused spot at z = L. By "turbulence-broadened, focused spot" we mean what Fante [9] calls the "short-term beam spread" for the focused beam. As Fante explains, long-scale turbulence

causes the beam to wander, while short-scale turbulence spreads it out. Thus the target receives a broadened, wandering spot (Figure 19).

Figure 19. Broadened, Wandering Spot

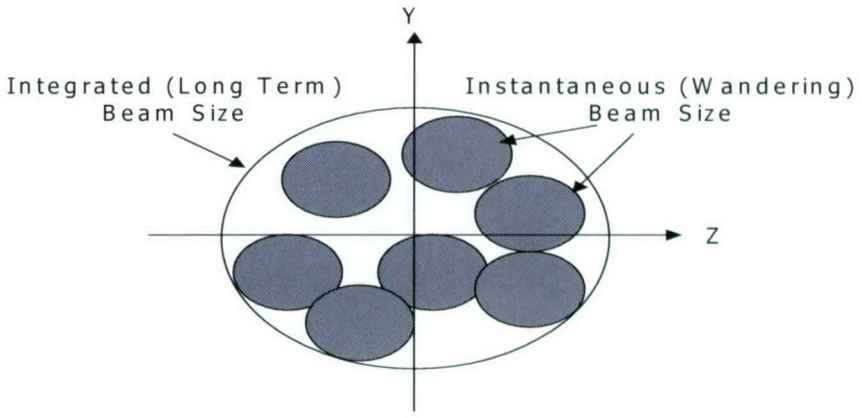

Source: after Fante [9], footnote 5.

We assume that the heating that causes blooming is influenced by the broadening, but not by the wandering.

Fante gives an expression for the radius of the broadened beam, ρ_s,

$$\rho_s = \frac{4L^2}{k_0^2 D^2} + \frac{4L^2}{k_0^2 \rho_f^2}\left(1 - 0.62\left(\frac{\rho_f}{D}\right)^{1/3}\right)^{6/5} \qquad \text{[Eq. 32]}$$

which we used. The parameter ρ_f in Equation 32 is equal to 48 percent of the parameter r_{os} evaluated in Equation 22.

Thus, we took

$$a(z) = D - (D - \rho_s)\frac{z}{L}. \qquad \text{[Eq. 33]}$$

which leads to

$$\frac{a(z)}{a_0} = 1 - \left(1 - \frac{\rho_s}{D}\right)\frac{z}{L} \qquad \text{[Eq. 34]}$$

To evaluate the iterated integral of Equation 31 with a single integral, we note that

$$\int_{z=0}^{L} \frac{a_0}{a(z)} \left[\int_{z'=0}^{z} \frac{a_0^2 w_0 \alpha(z') T_0}{a^2(z') w(z') \alpha_0 T(z')} dz' \right] dz = \int_{z'=0}^{L} \frac{a_0^2 w_0 \alpha(z') T_0}{a^2(z') w(z') \alpha_0 T(z')} \left[\int_{z=L}^{z'} \frac{a_0}{a(z)} dz \right] dz' \qquad \text{[Eq. 35]}$$

and that the integral with respect to z can be evaluated in closed form, as

$$\int_{z=L}^{z'} \frac{a_0}{a(z)} dz = \int_{z=L}^{z'} \frac{dz}{1-(1-\rho_s/D)z/L} = \frac{L}{1-\rho_s/D} \ln\left(\frac{1-(1-\rho_s/D)z'/L}{\rho_s/D} \right) \equiv g(z') \qquad \text{[Eq. 36]}$$

With the g(z′) determined in Equation 36, and using values of $T_0/T(z')$ from the 1976 U.S. Standard Atmosphere, we evaluated I_B numerically as

$$I_B = \int_{z'=0}^{L} \frac{a_0^2 w_0 \alpha(z') T_0}{a^2(z') w(z') \alpha_0 T(z')} g(z')\, dz' \qquad \text{[Eq. 37]}$$

WIND PROFILE

We needed to develop a wind profile w(z) that is realistic, and for which the integral of Equation 37 converges, and for which the Equation D.29 of the APS article [11] will apply. That equation, specifically,

$$\rho c_p w \frac{\partial T}{\partial x} = \alpha I \qquad \text{[Eq. 38]}$$

is the starting point of the blooming analysis of that reference.

For air-to-air engagements (except for shots made flying directly toward the target or away from it) the wind relative to the beam will be large along the entire path, Equation 38 will apply, and the integral will certainly converge.

But for a stationary target on the ground, it will not do simply to take the velocity profile generated by the motion of the beam from aircraft to a fixed ground target. That wind profile may fall linearly to zero at the target, and the integral of Equation 37 would not converge.

It is, however, possible that typical winds would be large enough for Equation 38 to apply. If so, then a simple profile w(z) that began with a speed like that of the weapon-bearing aircraft at z = 0, and fell to a typical surface wind speed at z = L, could be used.

We began our consideration of wind profile with the equation

$$\frac{\partial T}{\partial t} + \vec{q} \cdot \nabla T = \frac{k}{\rho c_p} \nabla^2 T + \frac{1}{\rho c_p} Q . \qquad \text{[Eq. 39]}$$

expressing conservation of energy in an isobaric motion of a fluid with constant specific heat at constant pressure c_p and thermal conductivity k, neglecting viscous dissipation. Equation 39 is written for an inertial frame moving with the beam *locally*. In Equation 39, $\vec{q}$ is fluid velocity in cm/sec, T is temperature in °K, Q denotes rate of heat addition in watts/cm^3, k is thermal conductivity in watts/(cm °K), and ρ is density in g/cm^3.

Introducing non-dimensional variables $\hat{T}$, $\hat{\vec{q}}$, $\hat{\vec{x}}$ and $\hat{t}$ with the definitions

$$\begin{aligned} \hat{t} &\equiv \frac{kt}{\rho c_p d^2} \\ \hat{\vec{q}} &\equiv \vec{q} / w \\ \hat{\vec{x}} &\equiv \vec{x} / d \\ \hat{T} &\equiv T / T_{ref} \end{aligned} \qquad \text{[Eq. 40]}$$

where $\vec{x}$ is position coordinate, w is fluid velocity relative to the beam, and d is beam diameter, brings Equation 39 to

$$\frac{k}{w \rho c_p d} \frac{\partial T}{\partial t} + \vec{q} \cdot \nabla T = \frac{k}{w \rho c_p d} \nabla^2 T + \frac{w}{d T_{ref}} Q \qquad \text{[Eq. 41]}$$

In Equation 41 we have suppressed the ^ symbols for clarity. Equation 40 shows that temperature changes will satisfy

$$\vec{q} \cdot \nabla T = \frac{w}{d T_{ref}} Q \qquad \text{[Eq. 42]}$$

provided that $\frac{k}{w \rho c_p d} << 1$, or, equivalently, that $w >> \frac{k}{\rho c_p d}$. For a representative case, $k = 2.55 \times 10^{-4}$ joule/(sec cm °K), $\rho = 1.225 \times 10^{-3}$ g/cm^3, $c_p = 1$ joule/(g °K), and the condition that Equation 41 governs temperature changes, and is $w >> 0.01$ cm/sec.

This condition is likely to be met by ordinary wind, even if the beam is fixed in space, as it would be on a stationary target on the ground.

With this result in mind, we developed the profile of wind relative to the beam in this way: If $\vec{V}_P$ and $\vec{V}_T$ denote respectively the velocity vectors of platform and

target, and if $\vec{W}$ denotes the wind velocity, then at a point on the beam located a fraction ς of the distance from platform to target, the beam will have velocity

$$\vec{V}(\varsigma) = \vec{V}_P + \varsigma(\vec{V}_T - \vec{V}_P) + \vec{W}(\varsigma)) \qquad \text{[Eq. 43]}$$

The magnitude V_{perp} of the velocity perpendicular to the beam will be given by the magnitude of the cross product of a unit vector parallel to the beam, and the beam's velocity $\vec{V}$. We evaluated that cross product, arbitrarily choosing the components of $\vec{W}$ to be a constant 2 m/s in each of 3 perpendicular directions, to obtain w(z).

In addition to parameters determined in evaluating I_B, evaluating B_0 required only a value for $\frac{1}{\rho_0}\frac{dn_0}{dT}$. We used the value -1×10^{-3} $cm^3/(g\ ^oK)$ given in the APS report cited above.

Blooming Results

With the approach described above, we found that blooming would reduce the range at which a surface target receives 1 kW per square centimeter from 71 km to about 58 km, a reduction of roughly 18 percent. In the case of 0.1 kw/cm^2, blooming reduced surface range only slightly, from 113 km to 112 km. The reason for this is that turbulence causes a larger spot size in the 0.1 kW/cm^2 case than it did in the case of 1 $kW/cm2$. There is less heating in the less-concentrated beam, and, consequently, less blooming.

Stable Secondary Atmospheric Motions

Long-range propagation through the atmosphere is certain to encounter turbulence. Also, as even casual observation of the sky will verify, stable, wave-like motions of the atmosphere are commonplace (Figure 20).

Figure 20. Atmospheric Waves, Made Visible by Clouds

We made only a preliminary consideration of the potential effects of atmospheric waves on airborne laser weapons. If (but only if) it is accurate to regard the waves as "frozen," that is, varying in time and space so slowly that our refracted-ray calculations give useful indications of the waves' effects on the laser beam, then those calculations may be used to study the displacement of the beam by atmospheric waves. We carried out a few such calculations, using the atmospheric wave model given by Wuertele et alii [12]. The results indicate that, for propagations over ranges of the order of 100 km, atmospheric waves might result in beam displacements on the order of one centimeter.

We believe that the effects of atmospheric waves on airborne laser weapons deserves more study than we were able to give it in this project.

SUMMARY AND CONCLUSIONS

Significant progress has been made during this year in both combat modeling and laser propagation modeling. The air-to-air and air-to-ground campaign analysis has addressed several ad hoc problems and has reached the point where the campaign model can be used for TACAIR analyses and decision making.

The air superiority campaign model, SLAACM, has been incorporated into an MS Excel / Visual Basic program. The current version of SLAACM models 4-ship Blue defense formations versus 12-ship Red attack packages. The Red packages include two 4-ship formations of escorts, protecting a 4-ship formation of bombers. There are quality options for both Blue and Red fighters and for Red bombers.

For each day of the campaign, Red assembles its attack packages to maximize its bombing effectiveness and the destruction of Blue forces. As a model option, Blue can respond randomly to the Red attack or use prior knowledge to preferentially attack the highest threat Red packages.

The model output includes

- updated daily listings of the Red order of battle,
- graphical depiction of Blue and Red fighter and Red bomber inventories, and
- tabulated values of targets destroyed and the tons of bombs delivered.

A campaign of several days runs in less than 1 minute on a Pentium 3 PC.

The laser analysis has reached the point where the propagation modeling is well understood and efficiently modeled. Addition of target interaction and scaling information related to high-energy laser systems must be addressed in future work to enable comparison of high-energy lasers with current air-to-air and air-to-ground weapons.

The laser propagation algorithms are incorporated in an MS Excel, Visual Basic workbook adequate for analysis, but have not yet been structured into a publishable model. Our current version models the 1.315 μ iodine laser with a limited number of atmospheric environments. The model runs quickly and produces tabular laser intensity and geometry data. Graphical data are also produced but are not updated run by run.

We plan to expand the model to include a solid state laser wavelength and additional atmospheric molecular and aerosol environments. Following clean-up of coding, implementation of improved input/output features and additional verification and validation, we intend to publish the model as the Airborne Laser Infrared Transmission (ALIRT) model.

Finally, we plan to investigate the use of the methods developed in the laser propagation analysis to investigate the performance requirements for laser rangefinders, laser designators, and electro-optical sensors both at independent sensors, and as part of a high-energy laser weapon system.

REFERENCES

[1] LMI, *Stochastic Models of Air Superiority Engagements and Campaigns*, Report PA104S1, David Lee, Scott Houser, Robert Hemm, and Jeremy Eckhause, June 2003.

[2] LMI, *Analytic Methods for the Studies of the Effectiveness of Tactical Aircraft*, Report PA201TR1, David Lee, Scott Houser, and Dou Long, June 30, 2003.

[3] F.W. Lanchester, *Aircraft in Warfare, The Dawn of the Fourth Arm* (Sunnyvale, CA: Lanchester Press, Inc., 1995) (originally published in 1916).

[4] Taylor, James G., *Lanchester Models in Warfare*, Volume I (Arlington, VA: Operations Research Society of America, March 1983).

[5] Taylor, James G., *Lanchester Models in Warfare*, Volume II (Arlington, VA: Operations Research Society of America, March 1983).

[6] R.J. Sasiela, *Electromagnetic Wave Propagation in Turbulence*, ISBN 0-387-57619-3 (New York, 1994).

[7] M.E Thomas and D.D. Duncan, *Atmospheric Transmission*, Chapter 1 of *Atmospheric Propagation of Radiation*, in Volume 2 of *The Infrared and Electro-Optical Systems Handbook*, F. G. Smith, Editor (copublished by The Infrared Information Analysis Center of the Environmental Institute of Michigan, Ann Arbor, and SPIE Optical Engineering Press, Bellingham, WA).

[8] Hugo Weichel, *Laser Beam Propagation in the Atmosphere*, Volume TT 3 (Bellingham, WA: SPIE Optical Engineering Press, 1990).

[9] R.L Fante, *Electromagnetic Beam Propagation in Turbulent Media*, Proc. IEEE 63, No. 12, December 1976. pp. 1669–1692.

[10] Robert Walter and Siva Mani, *Advanced Tactical Laser (ATL) Power-Aperture Trade Studies*, Laser Engineering and Technology Support (LETS), Schafer Corp., Task Order 0008, Contract F29601-98-D-0036, December 31, 2002.

[11] American Physical Society (APS), "*Report of the American Physical Society Study Group on Boost-Phase Intercept Systems for National Missile Defense*," July 2003.

[12] Weurtele et al., "Lee Waves, Benign and Malignant," NASA CR 186024, June 1993